Single-particle tracking of murine polyoma virus-like particles on live cells and artificial membranes

Helge Ewers*, Alicia E. Smith*, Ivo F. Sbalzarini†, Hauke Lilie‡, Petros Koumoutsakos†, and Ari Helenius*§

Institutes of *Biochemistry and †Computational Science, Swiss Federal Institute of Technology, CH-8093 Zurich, Switzerland; and ‡Institute of Biotechnology, Martin Luther University, D-06120 Halle, Germany

Edited by Harden M. McConnell, Stanford University, Stanford, CA, and approved August 26, 2005 (received for review May 27, 2005)

The lateral mobility of individual murine polyoma virus–like particles (VLPs) bound to live cells and artificial lipid bilayers was studied by single fluorescent particle tracking using total internal reflection fluorescence microscopy. The particle trajectories were analyzed in terms of diffusion rates and modes of motion as described by the moment scaling spectrum. Although VLPs bound to their ganglioside receptor in lipid bilayers exhibited only free diffusion, analysis of trajectories on live 3T6 mouse fibroblasts revealed three distinct modes of mobility: rapid random motion, confined movement in small zones (30–60 nm in diameter), and confined movement in zones with a slow drift. After binding to the cell surface, particles typically underwent free diffusion for 5–10 s, and then they were confined in an actin filament-dependent manner without involvement of clathrin-coated pits or caveolae. Depletion of cholesterol dramatically reduced mobility of VLPs independently of actin, whereas inhibition of tyrosine kinases had no effect on confinement. The results suggested that clustering of ganglioside molecules by the multivalent VLPs induced transmembrane coupling that led to confinement of the virus/receptor complex by cortical actin filaments.

gangliosides | lipid raft | total internal reflection fluorescence microscopy | virus entry | confinement zone

Dynamic events at the plasma membrane of live cells are commonly studied with light microscopy and single-particle tracking (SPT) after labeling of specific membrane components with individual fluorophores, colloidal gold, or fluorescent beads (1–3). Thorough analysis of the trajectories thus obtained provides information about the lateral mobility of membrane components and about the constraints imposed on them by cytoskeletal elements (4–6), cholesterol-rich microdomains (7, 8), and other structures that impose heterogeneity in the plasma membrane.

In this study, we have adopted this technology to analyze the lateral movement of incoming virus–like particles (VLPs) attached to their cell-surface receptors. The entry of animal viruses into their host cells starts with binding of the particles to lipids, proteins, or carbohydrates that serve as receptors on the cell surface. In many cases, binding is followed by receptor-mediated endocytosis of the virus and subsequent penetration of the viral capsid and accessory proteins from intracellular organelles into the cytosol (9). Although SPT has been used for virus entry (10, 11), the movement of virus particles on the cell surface before internalization has not been analyzed in detail.

Our study focused on murine polyoma virus (Py), a small (diameter, 45 nm), simple, nonenveloped DNA tumor virus (12) that uses gangliosides GD1a and GT1b as receptors (13) and relies on clathrin-independent, cholesterol-dependent endocytosis to deliver its genome into the cell for replication (ref. 14 and A.E.S., H.E., and A.H., unpublished observations). Instead of the infectious virus, we made use of VLPs that resemble the virus structurally but do not contain the DNA genome (15). These VLPs were assembled *in vitro* from recombinant viral protein 1, which was synthesized in *Escherichia coli*. Like intact viruses, VLPs bind via the viral protein 1 to the oligosaccharide moiety of the gangliosides and use them as entry receptors (16). Also like intact Py, the surface-bound VLPs activate tyrosine kinases and other signaling factors that induce endocytosis of the particles (ref. 17 and A.E.S., H.E., and A.H., unpublished observations).

Here, trajectories of individual, fluorescence-labeled VLPs on the surface of tissue culture cells and in artificial lipid bilayers were recorded with total internal reflection fluorescence (TIRF) microscopy for SPT. To analyze the trajectories quantitatively, the moment scaling spectrum (MSS) (18) was introduced as a computational method and used to categorize various modes of lateral motion. Typically, after binding to the cell surface, particles underwent free, cholesterol-dependent, lateral diffusion for a few seconds, rapidly followed by a period of confinement through an actin cytoskeleton-dependent mechanism.

Materials and Methods

Cell Culture and Reagents. 3T6 Swiss albino fibroblasts and mouse lung fibroblasts lacking expression of caveolin-1 (19) were grown in phenol red-free DMEM (GIBCO) supplemented with 10% FCS (LabForce, Nunningen, Switzerland), 4 mM GlutaMAX, and 50 mM Hepes (GIBCO) at 37°C in 5% CO_2. For live cell microscopy, cells were plated 24 h before experiments on 18-mm glass coverslips. The cells were transiently transfected using Nucleofector (Amaxa, Gaithersburg, MD). Plasmids encoding caveolin-1–GFP and clathrin light-chain–GFP have been described (20, 21). VLP purification, assembly (15), and labeling (16) are described in detail in *Supporting Materials and Methods*, which is published as supporting information on the PNAS web site.

Drug Treatments. The cells were incubated before VLP addition with the respective drugs as follows. Latrunculin A and jasplakinolide (Molecular Probes) were added for 15 min at 0.2 and 0.25 μM, respectively. To extract cholesterol from cells, serum-free medium supplemented with 10 mM methyl-β-cyclodextrin (MCD; Sigma) was used for 1 h. For cholesterol readdition, the medium was exchanged against serum-supplemented medium with 10 mM MCD–cholesterol complexes (Sigma) for 2 h. Genistein (Calbiochem) was added at 0.2 mM for 1 h. In all cases, the drugs were present during the experiment. The cellular cholesterol content was evaluated by using the Amplex red cholesterol assay kit (Molecular Probes).

Electron Microscopy. For negative staining, 0.4 μm mesh copper grids were coated with a 4-nm carbon film. A 10-μl sample

This paper was submitted directly (Track II) to the PNAS office.

Abbreviations: SPT, single-particle tracking; TIRF, total internal reflection fluorescence; VLP, virus-like particle; Fl-DPPE, fluorescein-dipalmitoylphosphatidylethanolamine; MCD, methyl-β-cyclodextrin; MSS, moment scaling spectrum; Py, polyoma virus; AF568, Alexa Fluor 568.

§To whom correspondence should be addressed at: Institute of Biochemistry, Schafmattstrasse 18, ETH Hoenggerberg, HPM E6.3, Swiss Federal Institute of Technology, CH-8093 Zurich, Switzerland. E-mail: ari.helenius@bc.biol.ethz.ch.

www.pnas.org/cgi/doi/10.1073/pnas.0504407102

containing 1 mg/ml VLPs was added for 30 s, drained of excess liquid, and stained for an additional 30 s with 2% uranyl acetate in distilled water. After transmission electron microscopy (EM 91 microscope, Zeiss), images were exported as 8-bit TIFF files and processed in PHOTOSHOP 7.0 (Adobe Systems, San Jose, CA).

SPT. Microscopy was performed on a custom modified Olympus IX71 inverted microscope as detailed in *Supporting Materials and Methods*. Live 3T6 cells on 18-mm coverslips were mounted in custom-made chambers. To avoid changes in membrane or cytoskeleton, the medium was not exchanged when mounting cells. VLPs were added at 0.1 μg/ml into the 0.5 ml of medium on the stage. Movies were recorded at a rate of 20 frames per s for 1,000 or 2,000 frames in TIRF mode. After each experiment, the cells that had been recorded were imaged by differential interference contrast microscopy to check for viability. Trajectories were harvested and analyzed by using a tracking program that we have developed (see ref. 22 and *Supporting Materials and Methods*). The position accuracy for the particles allowed by this program was on average 26 nm.

Internalization Assay. VLPs labeled with Alexa Fluor 568 (AF568) and FITC (Molecular Probes) were added to live cells at 37°C on the microscope stage. The fluorescent signal from both dyes was recorded at various intervals after VLP addition at a frame-rate of five per second. During recording, the medium was acidified to pH 4.5, resulting in a drastic shift in the FITC emission spectrum of particles exposed on the cell surface and loss of detectable fluorescence in the 505–530 nm channel. Fluorescence images were exported as 12-bit TIFF files, and processed in IMAGE J (National Institutes of Health, Bethesda).

Preparation of Artificial Lipid Bilayers. Artificial lipid bilayers were prepared by the vesicle drop method (23). Briefly, dioleoylphosphatidylcholine, fluorescein-dipalmitoylphosphatidylethanolamine (Fl-DPPE) (Avanti Polar Lipids) and GD1a (Hytest, Turku, Finland) were dissolved in chloroform:methanol (4:1), dried under nitrogen flow, and kept under vacuum for at least 2 h. The dried lipid mixture was resuspended in 50 mM Tris/0.2 M NaCl/2 mM $CaCl_2$, pH 7.4. Vesicles were formed by extrusion and added to plasma-cleaned glass coverslips. The resulting bilayer was rinsed five times to remove remaining vesicles. Before each SPT experiment on artificial bilayers, fluidity and continuity of the bilayer were assured by fluorescence recovery after photobleaching experiments of Fl-DPPE using a Zeiss LSM 510 confocal microscope as detailed in *Supporting Materials and Methods*.

Results

SPT of Py VLPs Bound to the Cell Surface. The VLPs used in this study were assembled from recombinant viral protein 1 pentamers (15). Sucrose gradient fractionation yielded a relatively homogenous population of particles, which electron microscopy after negative staining showed to have a Py-like appearance and a diameter of 43 ± 5 nm (Fig. 1*a*). Like the infectious viruses, they bound to GD1a, they were endocytozed and they inhibited infection when added together with the infectious virus to 3T6 cells (refs. 13, 16, and 17 and A.E.S., H.E., and A.H., unpublished observations). For visualization, FITC and/or AF568 were covalently coupled to the isolated VLPs. With an average of 182 fluorophores per particle, receptor–ligand interactions, and endocytosis of the VLPs remained unaltered (refs. 13 and 16 and A.E.S., H.E., and A.H., unpublished observations).

When the fluorescently labeled VLPs were added to live 3T6 cells on the microscope stage at 37°C, binding to the top surface could immediately be observed by epi-fluorescence microscopy (Fig. 1*b* and Movie 1, which is published as supporting information on the PNAS web site). After ≈15 min, VLPs in solution

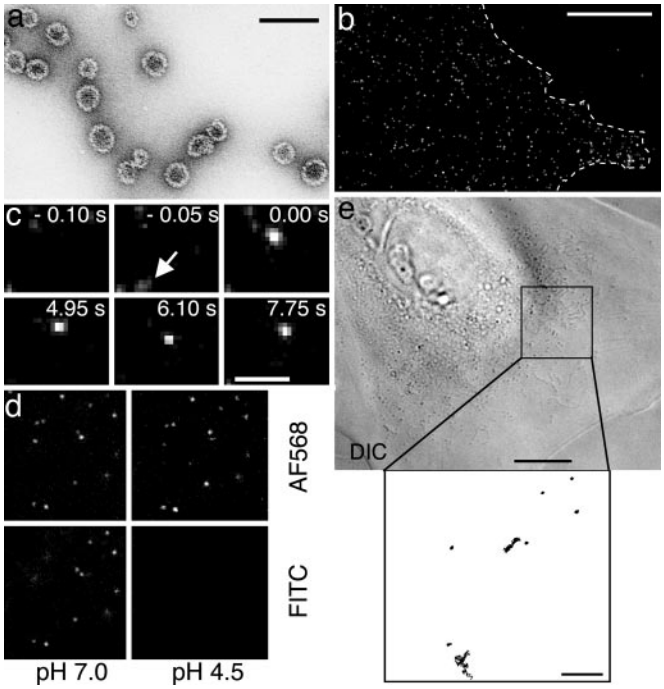

Fig. 1. SPT of Py VLPs on the bottom surface of live 3T6 cells. (*a*) Electron micrograph of VLPs visualized by negative staining. (Scale bar, 0.1 μm.) (*b*) Epi-fluorescence micrograph of AF568-labeled VLPs bound to a live 3T6 cell (Scale bar, 10 μm.) (*c*) TIRF microscopy images from a time series (20 Hz, 1,000 frames) showing a single AF568-labeled VLP binding to a 3T6 cell. The arrow points to the blurred particle fluorescence detected one frame before binding. (Scale bar, 1 μm.) (*d*) TIRF microscopy images of VLPs colabeled with FITC and AF568 and bound to the bottom surface of live 3T6 cells 45 min after VLP addition to the coverslip. The cells are in a medium at either pH 7.0 (*Left*) or pH 4.5 (*Right*). Note that the FITC emission spectrum shifts upon acidification, rendering the FITC fluorescence of acid-exposed VLPs undetectable. (*e*) (*Left*) Differential interference contrast (DIC) image of the cell shown in *d* acquired after acidification of the medium. (Scale bar, 10 μm.) (*Right*) The trajectories (20 Hz, 1,000 frames) of surface-bound VLPs were acquired by detecting AF568 before acidification. (Scale bar, 2 μm.)

drifted into the narrow space between the bottom surface of the cell and the cover glass and could be visualized by TIRF microscopy as rapidly moving, blurred, fluorescent objects. However, once bound to the bottom surface of a cell, they appeared as uniform, bright spots that were either stationary or laterally mobile. Fig. 1*c* and Movie 2, which is published as supporting information on the PNAS web site, show the binding and subsequent lateral diffusion of a single VLP recorded at high speed (20 Hz). First visible in the medium (Fig. 1*c*, arrow), the VLP can be seen to bind to the cell and to start moving laterally.

Because we were interested in the VLPs on the cell surface before endocytosis, it was important to define a window of time in which the particles recorded in TIRF microscopy were extracellular. To test whether particles were exposed to the external medium, we made use of VLPs that were double-labeled with AF568, which is not affected by pH, and with FITC, which is acid-sensitive. At varying intervals up to 60 min after VLP addition to cells, the media was acidified to pH 4.5 to quench the FITC fluorescence of extracellular VLPs. As illustrated in Fig. 1*d*, the FITC fluorescence signal of all particles recorded in TIRF microscopy 45 min after VLP addition was lost when the pH was lowered, indicating that the VLPs were still all extracellular. In recordings made at later time points, particles could occasionally be seen to undergo endocytosis; they disappeared from the evanescent field but remained visible by epi-fluorescence in both channels after acidification (data not

shown). We concluded that the cell-associated VLPs recorded by TIRF microscopy in the 15–45 min time period after virus addition were extracellular.

Mobility of Bound VLPs. For particle tracking, cells like the one shown in Fig. 1 *d* and *e* with several VLPs already bound were chosen and recorded in TIRF mode at 20 frames per s for a total of 50 or 100 s. Trajectories of particles were extracted from digital images by linking particle positions from frame to frame using a SPT algorithm (22). As illustrated by the trajectories of the eight VLPs in Fig. 1*e*, the motility of bound particles was heterogeneous. Some VLPs were virtually fixed in place, whereas others showed lateral movement covering areas of several microns-squared. To interpret the results, it was necessary to classify the trajectories by computational analysis.

Having collected 309 trajectories from 45 cells, the linear diffusion coefficient (D) was determined for each particle by a least-squares fit to the mean-square-displacement (MSD, $\langle r^2 \rangle$) plot as specified in *Supporting Materials and Methods*. The results indicated that many VLPs exhibited nonlinear diffusion. A measure of nonlinearity can be expressed by a parameter, α, indicating the nonlinear relationship of the MSD with time, $\langle r^2 \rangle = 4Dt^{\alpha}$ (24). Ferrari *et al.* (18) enhanced this measure by introducing an additional nonnegative, integer parameter ν such that $\langle r^{\nu} \rangle \sim t^{\gamma_{\nu}}$. The MSD is the special case, when $\nu = 2$, with $\gamma^{\nu} = \alpha$. The plot of γ^{ν} vs. ν is called the MSS, and its slope (S_{MSS}) yields a value that can be associated with a mode of motion characterizing the motility of the particles. There are two main advantages of the S_{MSS} method over the $\langle r^2 \rangle = 4Dt^{\alpha}$ classification: a smaller error because of the good linearity of the MSS and a clearer distinction between modes of motion (18) (*Supporting Materials and Methods*; see also Fig. 6, which is published as supporting information on the PNAS web site). An S_{MSS} value of 0.5 defines random, Brownian movement, whereas values below and above 0.5 are characteristic of confined and directed movement, respectively, with an S_{MSS} value of 0 for immobility.

By plotting D vs. S_{MSS} for the 309 VLPs, we could compare all trajectories in a single plot without arbitrary selection. The plot in Fig. 2*a* shows the combined data for all 309 trajectories. Three main modes of motion could be distinguished by the position in the D/S_{MSS} plot: (*i*) fast random motion ($D > 3 \times 10^{-3}$ μm^2/s, $S_{\mathrm{MSS}} \sim 0.5$), (*ii*) confinement to 30- to 60-nm diameter zones ($D < 2 \times 10^{-3}$ μm^2/s, $S_{\mathrm{MSS}} < 0.1$), and (*iii*) confinement with a slow drift ($D < 10^{-3}$ μm^2/s, $S_{\mathrm{MSS}} = 0.15$–0.35). When trajectories of drifting particles acquired at a 0.05-s frame-rate were averaged to 0.5-s intervals, they showed a macroscopic D of $0.5 - 1.5 \times 10^{-4}$ μm^2/s and a macroscopic S_{MSS} of 0.5 ± 0.1, indicating free but very slow diffusion. To facilitate assessment of the three main modes of motion, we have highlighted regions in the plot with boxes (Fig. 2*a*). The boxes included particles that displayed homogeneous mobility throughout the trajectory, and they excluded particles that showed composite modes of mobility and a few outliers that were confined to large areas (high D, low S_{MSS}) or diffused freely but slowly (low D, $S_{\mathrm{MSS}} \sim 0.5$). Directed movement of VLPs ($S_{\mathrm{MSS}} \gg 0.5$) was not observed.

Representative, full-length trajectories (Fig. 2*b*, trajectories 1, 2, and 3) for each mode of mobility and one of the composite trajectories (Fig. 2*b*, trajectory 4) are shown in Fig. 2*b* with the corresponding *xy* displacement, MSD, and MSS plots. The errors for the specific trajectories were calculated according to ref. 2. Note that the trajectories can be distinguished unambiguously when the MSD and MSS plots (Fig. 2*b*) are considered together.

Many of the points outside the boxes (exemplified by Fig. 2*b*, trajectory 4) exhibited heterogeneous behavior with periods of confinement interrupted by free diffusion. Several of such VLPs changed their mode of motion multiple times. In many cases, we observed that the particles visited the same confinement zone more than once, suggesting that the location of zones was a stable feature of the plasma membrane over periods up to 1–2 s. Furthermore, trajectories of VLPs recorded when bound to the top surface of cells by epi-fluorescence microscopy showed a similar distribution in the D/S_{MSS} plot as those at the bottom

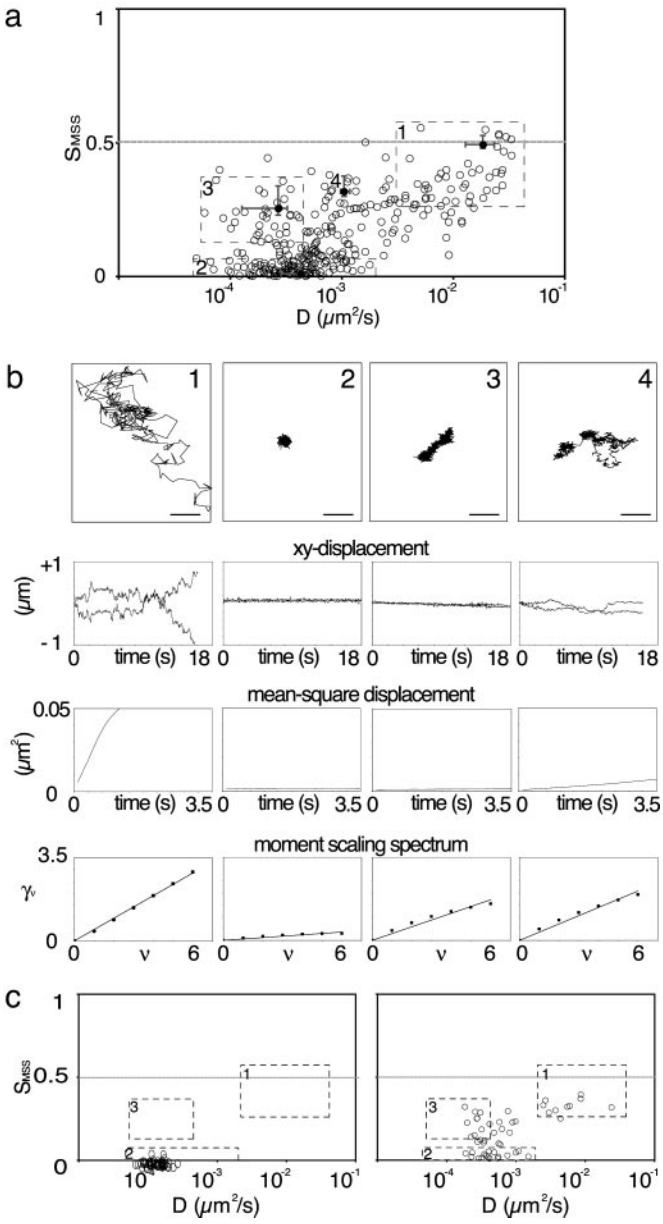

Fig. 2. Analysis of VLP trajectories from live cells. (*a*) Scatter plot of the diffusion coefficient versus the slope of the MSS (D/S_{MSS}) of VLP trajectories at the bottom surface of live cells. All harvested trajectories are plotted irrespective of the recorded length and whether the particles were bound or free at the start of the recording. Every point represents one trajectory and every trajectory is at least 100 steps (5 s) long. The longest trajectories are 2,000 steps (100 s) long. The three boxes highlight regions on the graph in which VLP motion is either rapid and random (box 1), confined (box 2), or confined with a slow drift (box 3). (*b*) Representative trajectories (numbered 1, 2, and 3) from each of the three boxes and one typical outlier (trajectory 4). The trajectories represent rapid and random movement (trajectory 1), confinement (trajectory 2) and confinement with a slow drift (trajectory 3). Trajectory 4 represents a VLP that changes its mode of motion during the acquisition time. Below each of these trajectories are the respective analytical plots: absolute displacement in μm for *x* and *y* direction versus time, MSD, and MSS. (*c*) D/S_{MSS} scatter plot of trajectories from control experiments performed with VLPs bound to glass coverslips (*Left*) or to the top surface of cells (*Right*).

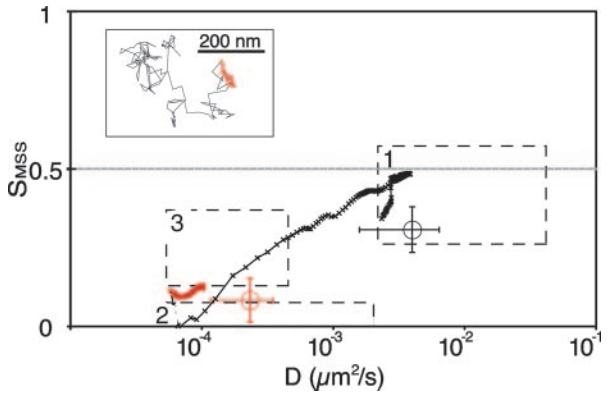

Fig. 3. Analysis of the mobility of binding particles. The D and S_{MSS} of particles imaged while binding to live cells were calculated separately for the mobile (black) and the confined (red) part of the trajectory ($n = 10$). The average positions on the D/S_{MSS} plot for the mobile and confined part are shown in the respective colors. To illustrate the sudden change in mobility, D and S_{MSS} were calculated for a moving window of 120 frames through the whole trajectory. The results of this analysis are graphed in a D/S_{MSS} plot, and the data points are connected according to time for better visibility (see also Movie 5).

surface ($n = 55$) (Fig. 2*c Right*). Thus, the mobility of VLPs bound to the bottom surface of cells was not affected by constraints caused by the confined space between cell and coverslip or by differences in cellular architecture between the top and bottom surfaces.

Mobility in Artificial Lipid Bilayers. To determine the limit of detection of surface mobility, VLPs were bound to coverslips in the absence of cells and tracked under conditions identical to the experimental ($n = 50$). These immobilized VLPs defined the slowest observable mobility with a D of $1.31 \pm 0.40 \times 10^{-4}$ $\mu m^2/s$. An average S_{MSS} of these particles of below zero indicated that their mobility was below the threshold set by camera noise (Fig. 2c *Left*). All trajectories of VLPs on cells with an $S_{MSS} < 0$ were omitted from further analysis.

To obtain information about unconstrained diffusion of VLPs, we recorded trajectories of VLPs bound to artificial lipid bilayers at 37°C. The bilayers were generated on the surface of glass coverslips by deposition of small unilamellar liposomes (23). The liposomes were composed of dioleoylphosphatidylcholine, with 0.07 mole % of GD1a and 1 mole % of FL-DPPE. To confirm that the bilayers were fluid and continuous, fluorescence recovery after photobleaching experiments of the FL-DPPE were performed at room temperature before each SPT experiment (Fig. 7 *a* and *b* and Movie 3, which are published as supporting information on the PNAS web site). A diffusion coefficient (D) of 3.96 ± 0.82 $\mu m^2/s$ ($n = 7$) was determined for FL-DPPE in agreement with published observations (25). The VLPs did not bind to control bilayers devoid of GD1a (data not shown). When GD1a was present, the VLPs attached to the bilayers, and moved rapidly in the plane of the membrane (Movie 4, which is published as supporting information on the PNAS web site). They exhibited a D of 0.032 ± 0.023 $\mu m^2/s$, and a S_{MSS} of 0.42 ± 0.096 ($n = 39$), indicating free diffusion (Fig. 7*c*). It was apparent that VLPs were slightly more mobile in these artificial membranes than during free diffusion in the 3T6 plasma membrane. Also, VLPs frequently detached from the bilayers in contrast to cellular membranes where dissociation was not observed.

Confinement. When VLPs were tracked from the moment of binding onward, it became clear that free diffusion, as a rule, preceded confinement. For 12 of 18 particles analyzed in this way, the period of initial rapid, random motion lasted 5–10 s. The loss of mobility that followed this period was sudden; it occurred between two frames (50 ms). The dramatic change in mobility also could be demonstrated by calculating the D and S_{MSS} in a moving window of 120 frames through the trajectory (Fig. 3 and Movie 5, which is published as supporting information on the PNAS web site). Escape from confinement, when it happened, was equally rapid. When the rapid change in mobility was used as a dividing point, D and S_{MSS} could be calculated separately for the mobile and immobile parts of the trajectories. Immediately after stable binding, the VLPs showed relatively high D and S_{MSS} as expected for free diffusion (Fig. 3, box 1). In contrast, VLPs showed a much lower D and a S_{MSS} of <0.2 after the sudden loss of mobility, indicative of subdiffusive motion (Fig. 3, boxes 2 and 3).

The confinement zones observed for VLPs in 3T6 cells fell into a size range of 500–3,000 nm^2. To determine whether the confinement zones corresponded to clathrin-coated pits or caveolae, VLPs were added to cells transiently expressing clathrin light-chain–GFP or caveolin-1–GFP. Published studies with both GFP constructs and our own observations showed that they are functional in endocytosis and membrane trafficking (20, 21). Movies of the GFP-tagged proteins and VLPs were acquired by two-color TIRF microscopy.

No VLPs were found to colocalize with, or move into, clathrin light-chain–GFP- or caveolin-1–GFP-positive areas in the plasma membrane (Fig. 4 *a* and *b*; see also Movies 6 and 7, which is published as supporting information on the PNAS web site).

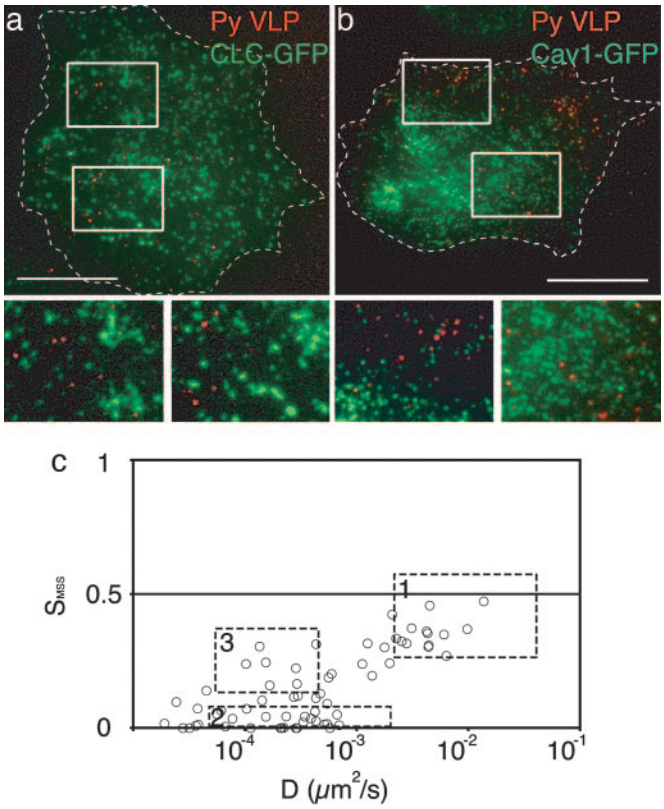

Fig. 4. Confinement of VLPs on the cell surface does not require caveolae or clathrin-coated pits. TIRF images of AF568 VLPs bound to the bottom surface of live 3T6 cells expressing clathrin light chain–GFP (*a*) or caveolin-1–GFP (*b*). (Scale bars, 10 μm.) For each construct, a representative merged, dual-color image of a whole cell (*Upper*) and close-ups (insets in *Upper* shown in *Lower*) are shown. (c) D/S_{MSS} plot of VLP trajectories from particles bound to lung fibroblasts obtained from caveolin-1 knockout mice.

CELL BIOLOGY

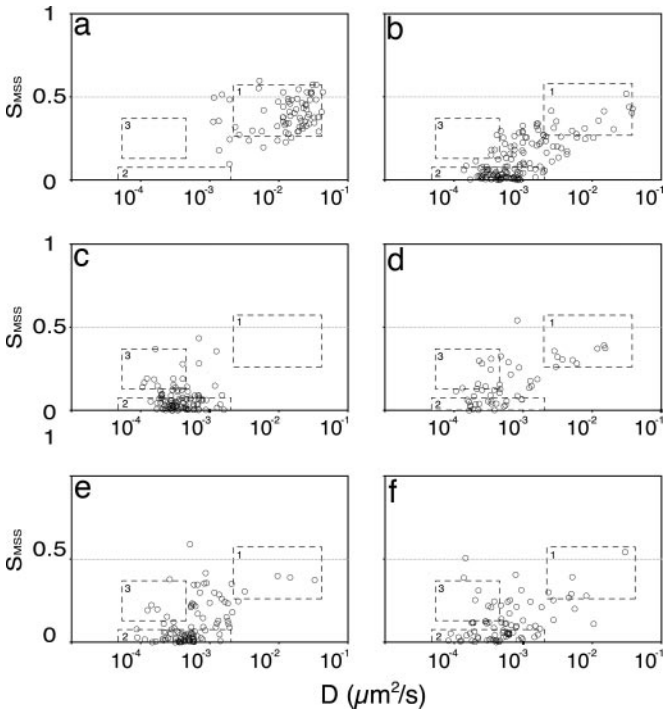

Fig. 5. Effect of perturbations of cellular actin and cholesterol on VLP motion. D/S_{MSS} plots show VLP mobility when bound to cells in the presence of 0.2 μM latrunculin A added 15 min before the VLPs (*a*), 0.25 μM jasplakinolide added in the same way (*b*), 10 mM MCD added 1 h before the VLPs (*c*), 10 mM MCD–cholesterol complex added for 2 h to cells pretreated with MCD as in *c* (*d*), 0.2 μM latrunculin A for 15 min in cells pretreated as in *c* (*e*), and 0.2 mM genistein for 1 h added before the VLPs (*f*).

When we analyzed the surface mobility of VLPs on primary fibroblasts derived from caveolin-1-null mice (19), confinement occurred as frequently as in the 3T6 cells, and the overall distribution of mobilities in the D/S_{MSS} plot did not differ (Fig. 4*c*) ($n = 75$). Thus, consistent with our findings that Py endocytosis and infection are independent of clathrin- and caveolae-mediated endocytosis (A.E.S., H.E., and A.H., unpublished observations), confinement of VLPs did not involve entrapment in clathrin-coated pits or surface caveolae.

To determine whether the actin cytoskeleton was responsible for VLP confinement, the effects of inhibitors of actin filament assembly and disassembly were tested. Mild inhibition of microfilament assembly by low concentration of latrunculin A (200 nM) resulted in virtually complete loss of VLP confinement ($n = 74$) (Fig. 5*a*). At this concentration, TIRF microscopy using actin–GFP-expressing 3T6 cells showed that cortical actin was disorganized, whereas stress fibers were still intact (Movie 8, which is published as supporting information on the PNAS web site). Jasplakinolide, which inhibits microfilament disassembly, did not affect free diffusion and confinement. The drift often observed in control cells was abolished ($n = 146$) (Fig. 5*b*). We concluded that after a period of free diffusion, the VLP particles were limited in lateral movement by the cortical actin network. Once trapped by this network, VLP movement was limited to local shifts permitted by dynamic changes in the constraining filaments.

The Effects of Cholesterol Depletion and Kinase Inhibition. VLP internalization and Py infectivity are inhibited by cholesterol depletion and inhibition of tyrosine kinases (ref. 14 and A.E.S., H.E., and A.H., unpublished observations). To determine whether cholesterol was important for VLP mobility on the cell surface, we reduced cellular cholesterol levels to <40% using the cholesterol-depleting drug MCD. Strikingly, VLPs bound to these cells did not exhibit free diffusion at any time (Fig. 5*c*) ($n = 256$). Similar results were obtained after depletion of cholesterol by overnight incubation with nystatin and progesterone. The immobilization effect was reversible because after readdition of cholesterol to the cells, the distribution of VLP mobilities was again similar to that of untreated cells ($n = 68$) (Fig. 5*d*). The loss of free diffusion after cholesterol depletion was independent of cortical actin because addition of latrunculin A to cholesterol-depleted cells did not restore free mobility to the majority of VLPs ($n = 102$) (Fig. 5*e*).

In contrast, the tyrosine kinase inhibitor genistein, which also blocks Py entry into cells, had no detectable effect on VLP confinement when added 1 h before the SPT experiments ($n = 101$) (Fig. 5*f*). We concluded that tyrosine kinases were not required for free diffusion or confinement of VLPs.

Discussion

When the trajectories of cell-bound VLPs were analyzed by using the diffusion constant and MSS, different modes of motion could be distinguished. Immediately after binding, the VLPs displayed 5–10 s of rapid, random diffusion at a rate only marginally slower than observed for VLPs bound to the ganglioside receptor GD1a in dioleoylphosphatidylcholine bilayers. The free diffusion ended in an abrupt decrease in mobility, and the particles were now confined to areas with a diameter of 30–60 nm. Some VLPs continued to display a slow, random drift. Occasionally, VLPs broke loose again and entered another phase of free diffusion, only to be trapped again in the same or different confinement zones.

The zones to which the VLPs were confined did not overlap with clathrin-coated pits or caveolae, and the process of confinement did not seem to be directly linked to endocytosis. The particles could, in fact, be confined for up to half an hour or more before endocytic internalization, and the tyrosine kinase-induced signals needed to initiate endocytosis were not required for confinement. Moreover, we have found that dissociation of actin filaments by latrunculin A, which prevented confinement, did not affect either VLP endocytosis or Py infection in the same cell type (A.E.S., H.E., and A.H., unpublished observations). Thus, it seems likely that the confinement of VLPs reflected a basic property of the plasma membrane and may be attributed to the general phenomenon of compartmentalization of the membrane by the cytoskeleton (26).

On the basis of SPT and fluorescence recovery after photobleaching studies, several groups have concluded that the plasma membrane is partitioned by actin filaments on the cytosolic surface into nanocompartments that allow rapid local diffusion of proteins and lipids within them but suppress long-range diffusion that involves intercompartment movement (4, 6, 26). To explain the effects of cortical actin, a membrane skeleton "fence" or "corral" model and an anchored-transmembrane protein "picket" model (4, 5, 27, 28) have been proposed.

The fence or corral scenario involves partitioning of the cytosolic surface of the plasma membrane by tightly apposed dynamic actin filaments forming a grid on the inside surface. The filaments prevent free diffusion of proteins and complexes with bulky cytoplasmic protrusions. Although such proteins and complexes are free to diffuse within each partition of the grid, intercompartment movement is restricted (4, 6, 26, 29, 30). In the picket scenario, bulky cytoplasmic domains are not required for confinement. Rather, transmembrane proteins fixed in place by cortical actin filaments act as obstacles of lateral mobility for components in both membrane leaflets. The magnitude of the constraints imposed by such pickets depends on the size of the mobile entities and on the degree of crowding (5).

In the case of VLPs, the ganglioside receptors to which they bind are confined to the outer bilayer leaflet. It is not obvious how the transmembrane coupling that leads to actin-mediated confinement occurs in this case. However, because individual glycan moieties of gangliosides associate with a binding constant of less than millimolar to viral protein 1 (31), it is likely that the VLPs are anchored by multiple gangliosides from the very beginning (32). Clustering of gangliosides using cholera toxin β subunit has been shown to induce phase separation in artificial lipid bilayers (33). Furthermore, gangliosides as well as cell-surface-associated VLPs localize to the detergent-resistant fraction of the membrane (ref. 34 and A.E.S., H.E., and A.H., unpublished observations). Taken together, these findings lead to the conclusion that VLP–ganglioside complexes are part of lipid rafts (7) that may be a key step in transmembrane coupling and subsequent entrapment.

We found that the initial phase of free diffusion was eliminated by depletion of cellular cholesterol, a treatment that blocks endocytosis of VLPs and inhibits Py infection (ref. 14 and A.E.S., H.E., and A.H., unpublished observations). That cholesterol depletion would lead to immobilization of plasma membrane components is not unprecedented in the literature. A reduction in lateral mobility of several glycosylphosphatrdylinositol-anchored proteins, transmembrane proteins, and lipids has been reported (35–38). One mechanism put forward to explain the effect is actin-independent, reversible agglutination of lipids into large, stable, ordered lipid domains (35, 36, 38). In contrast, it has been proposed that cholesterol depletion causes a drop in the $PI(4,5)P_2$-level, which in turn affects the cortical actin cytoskeleton and thus lowers lateral mobility of membrane components (37). Because latrunculin A did not reverse the effect of cholesterol depletion, the lack of VLP mobility in cholesterol-depleted cells was most likely due to the formation of large immobile membrane patches containing the gangliosides and the bound VLPs.

For Py VLPs, our results lead us to a model that begins with binding of the incoming VLP to the oligosaccharide moieties of several ganglioside molecules. The lateral mobility of the complex thus formed is not constrained until some form of transbilayer coupling occurs that imposes strict, actin filament-dependent confinement on the VLP–receptor complex. The change is most likely caused by the addition of further components to the complex. These components may form a direct bridge to the actin filaments, or a change in size or structure of the complex alone may suffice for it to become constrained either through the fence or the picket mechanism. Because the slow drift often observed after confinement of VLPs was reduced by jasplakinolide treatment, it is likely that the full complex can move from one nanocompartment to the next but only as long as the filament lattice is dynamic and subject to local rearrangement. The occasionally observed rapid return of VLPs to free diffusion may represent destabilization of the complex.

Regardless of whether the complex is trapped by actin or not, kinases and other signaling factors are recruited and proceed to turn on a cascade that eventually leads to the endocytic internalization of the VLPs. Further work on the behavior of cell bound viruses and VLPs by using SPT, TIRF microscopy, and other methods that provide dynamic information about cell-surface processes will help to clarify the significance and generality of these effects and will help us to understand the properties of the plasma membrane.

We thank J. Kartenbeck for electron microscopy, G. Csucs and F. Rossetti for helpful discussions, P. Deprez for helpful comments on the manuscript, and all members of the A.H. laboratory for support. This work was supported by Swiss Federal Institute of Technology Grant TH-1/02-2 (to A.H. and P.K.), Deutsche Forschungsgemeinschaft Grant SFB 610 (to H.L.), and Human Frontier Science Program Grant LT00793/2003 (to A.E.S.).

1. Saxton, M. J. & Jacobson, K. (1997) *Annu. Rev. Biophys. Biomol. Struct.* **26,** 373–399.
2. Qian, H., Sheetz, M. P. & Elson, E. L. (1991) *Biophys. J.* **60,** 910–921.
3. Vrljic, M., Nishimura, S. Y., Brasselet, S., Moerner, W. E. & McConnell, H. M. (2002) *Biophys. J.* **83,** 2681–2692.
4. Sako, Y. & Kusumi, A. (1994) *J. Cell Biol.* **125,** 1251–1264.
5. Kusumi, A., Nakada, C., Ritchie, K., Murase, K., Suzuki, K., Murakoshi, H., Kasai, R. S., Kondo, J. & Fujiwara, T. (2004) *Annu. Rev. Biophys. Biomol. Struct.* **34,** 351–378.
6. Edidin, M., Kuo, S. C. & Sheetz, M. P. (1991) *Science* **254,** 1379–1382.
7. Simons, K. & Ikonen, E. (1997) *Nature* **387,** 569–572.
8. Dietrich, C., Yang, B., Fujiwara, T., Kusumi, A. & Jacobson, K. (2002) *Biophys. J.* **82,** 274–284.
9. Smith, A. E. & Helenius, A. (2004) *Science* **304,** 237–242.
10. Babcock, H. P., Chen, C. & Zhuang, X. (2004) *Biophys. J.* **87,** 2749–2758.
11. Seisenberger, G., Ried, M. U., Endress, T., Buning, H., Hallek, M. & Brauchle, C. (2001) *Science* **294,** 1929–1932.
12. Stehle, T., Yan, Y., Benjamin, T. L. & Harrison, S. C. (1994) *Nature* **369,** 160–163.
13. Tsai, B., Gilbert, J. M., Stehle, T., Lencer, W., Benjamin, T. L. & Rapoport, T. A. (2003) *EMBO J.* **22,** 4346–4355.
14. Gilbert, J. & Benjamin, T. (2004) *J. Virol.* **78,** 12259–12267.
15. Gleiter, S. & Lilie, H. (2001) *Protein Sci.* **10,** 434–444.
16. Smith, A. E., Lilie, H. & Helenius, A. (2003) *FEBS Lett.* **555,** 199–203.
17. Richterova, Z., Liebl, D., Horak, M., Palkova, Z., Stokrova, J., Hozak, P., Korb, J. & Forstova, J. (2001) *J. Virol.* **75,** 10880–10891.
18. Ferrari, R., Manfroi, A. J. & Young, W. R. (2001) *Physica D* **154,** 111–137.
19. Drab, M., Verkade, P., Elger, M., Kasper, M., Lohn, M., Lauterbach, B., Menne, J., Lindschau, C., Mende, F., Luft, F. C., *et al.* (2001) *Science* **293,** 2449–2452.
20. Pelkmans, L., Kartenbeck, J. & Helenius, A. (2001) *Nat. Cell Biol.* **3,** 473–483.
21. Gaidarov, I., Santini, F., Warren, R. A. & Keen, J. H. (1999) *Nat. Cell Biol.* **1,** 1–7.
22. Sbalzarini, I. F. & Koumoutsakos, P. (2005) *J. Struct. Biol.* **151,** 182–195.
23. Groves, J. T., Boxer, S. G. & McConnell, H. M. (1997) *Proc. Natl. Acad. Sci. USA* **94,** 13390–13395.
24. Feder, T. J., Brust-Mascher, I., Slattery, J. P., Baird, B. & Webb, W. W. (1996) *Biophys. J.* **70,** 2767–2773.
25. Derzko, Z. & Jacobson, K. (1980) *Biochemistry* **19,** 6050–6057.
26. Sheetz, M. P., Schindler, M. & Koppel, D. E. (1980) *Nature* **285,** 510–511.
27. Edidin, M. (1992) *Trends Cell Biol.* **2,** 376–380.
28. Schlessinger, J., Elson, E. L., Webb, W. W., Yahara, I., Rutishauser, U. & Edelman, G. M. (1977) *Proc. Natl. Acad. Sci. USA* **74,** 1110–1114.
29. Ritchie, K., Shan, X. Y., Kondo, J., Iwasawa, K., Fujiwara, T. & Kusumi, A. (2005) *Biophys. J.* **88,** 2266–2277.
30. Murase, K., Fujiwara, T., Umemura, Y., Suzuki, K., Iino, R., Yamashita, H., Saito, M., Murakoshi, H., Ritchie, K. & Kusumi, A. (2004) *Biophys. J.* **86,** 4075–4093.
31. Stehle, T. & Harrison, S. C. (1996) *Structure (London)* **4,** 183–194.
32. Herrmann, M., von der Lieth, C. W., Stehling, P., Reutter, W. & Pawlita, M. (1997) *J. Virol.* **71,** 5922–5931.
33. Hammond, A. T., Heberle, F. A., Baumgart, T., Holowka, D., Baird, B. & Feigenson, G. W. (2005) *Proc. Natl. Acad. Sci. USA* **102,** 6320–6325.
34. Ortegren, U., Karlsson, M., Blazic, N., Blomqvist, M., Nystrom, F. H., Gustavsson, J., Fredman, P. & Stralfors, P. (2004) *Eur. J. Biochem.* **271,** 2028–2036.
35. Vrljic, M., Nishimura, S. Y., Moerner, W. E. & McConnell, H. M. (2005) *Biophys. J.* **88,** 334–347.
36. Kenworthy, A. K., Nichols, B. J., Remmert, C. L., Hendrix, G. M., Kumar, M., Zimmerberg, J. & Lippincott-Schwartz, J. (2004) *J. Cell Biol.* **165,** 735–746.
37. Kwik, J., Boyle, S., Fooksman, D., Margolis, L., Sheetz, M. P. & Edidin, M. (2003) *Proc. Natl. Acad. Sci. USA* **100,** 13964–13969.
38. Hao, M., Mukherjee, S. & Maxfield, F. R. (2001) *Proc. Natl. Acad. Sci. USA* **98,** 13072–13077.